Local order in two-dimensional colloidal aggregation

J. C. Earnshaw, M. B. J. Harrison, and D. J. Robinson*
The Department of Pure and Applied Physics, The Queen's University of Belfast, Belfast BT7 1NN, Northern Ireland
(Received 7 December 1995)

Diffusion limited cluster-cluster aggregation in two dimensions has been studied both experimentally and in computer simulation. In both cases the structure function at late times exhibits hitherto unsuspected sixfold symmetry. The triangular structure of the system in real space is not very pronounced, resembling the local order of a liquid. The six peaks in the structure function lie at the wave number of the characteristic spatial modulation previously found for this system. It is argued that both phenomena arise due to mutually exclusive depletion zones which form around clusters in diffusion limited aggregation, providing an effective long-range intercluster repulsion. [S1063-651X(96)03906-2]

PACS number(s): 82.70.−y

I. INTRODUCTION

Spatial or temporal pattern formation is a common feature of systems driven far from equilibrium [1,2]. Such self-organization has been observed in systems ranging from the physical to the biological, including oscillatory chemical reactions [3] and brain activity [4]. However, apart from such limiting cases as periodic lattices and entirely random structures, spatial pattern or order is not readily describable [1]. Symmetry provides a useful measure in at least some cases. We have discovered, surprisingly, that hexagonal symmetry spontaneously forms in certain cases of random colloidal aggregation. In this example of pattern formation order emerges in competition with the growth of irregular, fractal structures, which is more commonly associated with the *destruction* of order far from equilibrium [1].

The aggregation of small particles to form large clusters is a process of fundamental interest in many diverse branches of science, and has long been an active area of scientific interest. We have studied cluster-cluster aggregation in two-dimensional (2D) systems both experimentally [5–7] and by computer simulation. The experimental system comprises electrically charged, micrometer-sized polystyrene spheres trapped on the surface of water. Addition of salt to the subphase screens the charge so that the particles can approach close enough for van der Waals attraction to cause apparently irreversible bonding. Two-dimensional colloidal systems have several attributes that make them particularly useful. They provide an experimentally convenient approach to a two-dimensional system, in which, in principle, the interparticle interactions can be modified to cause either reaction limited cluster-cluster aggregation (RLCA), in which the probability of two particles bonding on contact is significantly less than 1, or the diffusion limited case (DLCA), in which this probability is essentially unity. Particular advantages for the present work include: the high density limit of cluster-cluster aggregation can be realized and studied more easily than in three dimensions, phase separation under the action of gravity is precluded, and the aggregates are less liable to mechanical instability induced by bending or hydrodynamic stress.

Most recent studies of aggregation, influenced by the ideas of fractal geometry, have concentrated on the structure of the clusters [8] and on the kinetics [9]. However, in the case of diffusion limited cluster-cluster aggregation certain recent studies [10–12] have revealed the emergence of collective aspects of the system, implying the existence of intercluster spatial order in these nonequilibrium systems. This order manifests itself in scaling or stationarity of various properties of the system throughout aggregation [13,14]. The underlying intercluster order, which extends beyond the scale of the fractal clusters, arises from self-organization due to interactions between the growing clusters. In this paper we report aspects of this order, revealing the spontaneous breaking of rotational symmetry by this self-organization.

The principal results presented here derive from the experimental study. They are, however, supported in essentially every respect by the simulations, data from which are touched on briefly. The paper is organized as follows: the next section summarizes the methods used in both experiment and simulation, Sec. III presents the data and argues the reality of the effects observed and in Sec. IV we discuss the mechanism underlying the observed order, draw an analogy with local order in liquids, and connect the present results with various other aspects of the system studied.

II. METHODS

A. Experiment

Our experimental methods have been described in full elsewhere [5]. In brief, polystyrene latex spheres of diameter 1.09 ± 0.08 μm were spread on the surface of an aqueous subphase, where they remained securely trapped. They are highly charged and interact via long-range electrostatic forces [15]. Adding salt ($CaCl_2$) to the subphase induced aggregation, which proceeded to gelation over times of the order of 2–3 h. Times were measured from the initiation of aggregation by addition of salt to the aqueous subphase. Images (768×512 pixel^2, 0.95 μm/pixel) were grabbed at various stages (usually every 15 min) throughout aggregation

*Present address: Andor Technology, The Queen's University, Belfast BT7 1NN, Northern Ireland.

for subsequent analysis. Such sequences of images represent quasirandomly selected samples, due to some mobility of the colloidal monolayers [5].

Monolayer area fractions (ϕ) were rather high, typically ≈ 0.1. For much lower ϕ aggregation took many hours, during which the aqueous subphase evaporated, so changing the salt concentration and thus the aggregation conditions. At much higher ϕ it was difficult, if not impossible, to form a homogeneous monolayer during the spreading process. We have thus explored only a modest range of area fractions; in comparable stages of aggregation in all experiments the phenomena were similar.

A typical monolayer comprises $\sim 5\times 10^7$ spheres, so that finite size effects should be negligible for the system as a whole. Typically, each micrograph contains some 10^5 particles. While this number is reasonably large, the statistics of present interest relate to the cluster numbers, which are much smaller.

B. Simulation

The computer simulations used a 2D square lattice (1024×1024), with periodic boundary conditions. Particles (of size one lattice square) were placed at randomly chosen lattice sites. The number of particles was determined by the required area fraction, here taken as 0.1 to be comparable with the experimental values. If any two or more of the initial lattice sites occupied by particles were adjacent, these particles were joined to form a cluster. After this initialization, the aggregation process was started. Particles or clusters were chosen at random and moved by one lattice step in a randomly chosen direction. The diffusion coefficient was thus taken to be mass-independent; the results to be described are not affected by this assumption, but the simulations ran significantly faster. If such a move brought two particles or clusters into contact the two were joined rigidly and the combined object subsequently moved as a single cluster. Time was incremented by $1/N(t)$ at each move, $N(t)$ being the total number of separate objects (monomers and clusters) in the system at time t. The simulations were run until gelation.

III. RESULTS

We present representative experimental data before briefly considering results from computer simulations.

A. Experimental study

Above a critical $CaCl_2$ concentration ($\sim 0.5M$) the structure of the fractal clusters resembled that expected for diffusion limited cluster-cluster aggregation [5]. Below this concentration the cluster structure corresponded to the reaction limited case. In both cases the growth kinetics showed a crossover from slow to rapid aggregation as time progressed (Fig. 1) [6]. The DLCA-like fractal scaling at high $CaCl_2$ concentrations only appeared after this crossover [7]. We restrict ourselves to discussion of the phenomena at high salt concentrations, and specifically the DLCA situation.

Figure 2 shows a typical sequence of binary images of the aggregating colloidal monolayer for a particular experiment. The center 512×512 portion of the binarized images was

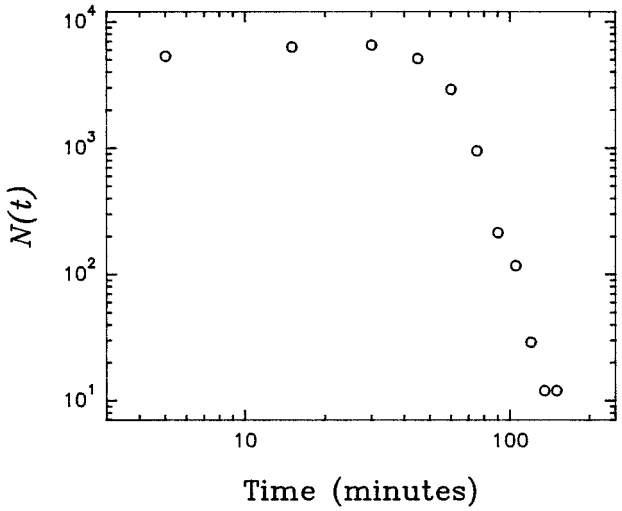

FIG. 1. The number of clusters within the micrographs at various times after initiation of aggregation in an experiment on a $0.73M$ $CaCl_2$ subphase. Note the crossover from slow to rapid growth at about 45 min.

analyzed to provide the structure function (or, in image analysis terms, the power spectrum) of the monolayer:

$$S(\mathbf{q},t)\propto\left|\int \rho(\mathbf{r},t)e^{i\mathbf{q}\cdot\mathbf{r}}d\mathbf{r}\right|^2, \tag{1}$$

where $\rho(\mathbf{r},t)$ is the local density. The two-dimensional structure function was azimuthally averaged to give $S(q,t)$. The absolute magnitudes of the computed $S(q,t)$, while similar, were slightly different for individual images because of the statistical variations in the number of particles present. We thus normalized the structure functions to a common value at an arbitrary large value of q ($3.88\ \mu m^{-1}$), beyond the range of interest.

Under the present aggregation conditions the particle density in the system is modulated by a particular wavelength [12]. Figure 3 shows the angularly averaged structure functions for the experiment corresponding to Fig. 2. The principal feature of these functions is the peak (ring in 2D) which is present (at wave number q_m) at all times. The fractal scaling in $S(q,t)$ is only apparent above q_m, which thus corresponds to a characteristic distance beyond which the fractal scaling breaks down. In the DLCA regime (i.e., after the crossover at 45 min) the structure functions scale as

$$S(q/q_m,t)=q_m^{-d}(t)F(q/q_m), \tag{2}$$

where the exponent d equals the fractal dimension d_f, and the function $F(q/q_m)$ is a time-independent function whose character continues to excite discussion [16,17]. Similar results have been reported for dense colloidal suspensions in three dimensions [10]. As has been pointed out by Carpineti and Giglio [10], a scaling exponent equal to d_f is trivially necessary if the fractal power-law decay of $S(q,t)$ at $q>q_m$ is to be preserved. Such scaling has more generally been associated with the late stages of spinodal decomposition [18], where the exponent d is just the dimensionality of the space in which the system is embedded.

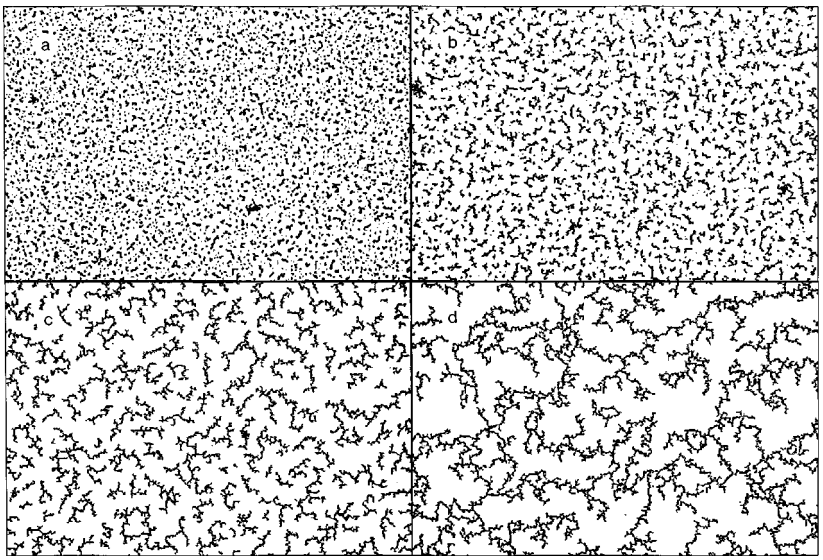

FIG. 2. Video micrographs of an aggregating monolayer of 1 μm polystyrene spheres on the surface of an aqueous 0.73M $CaCl_2$ solution. The images are 768×512 pixels^2, one pixel $\equiv0.95$ μm. The images correspond to $t=60$ (a), 75 (b), 105 (c), and 135 min (d).

The angular averaging of $S(q,t)$ as shown in Fig. 3 conceals a rather remarkable feature of the 2D structure function. Figure 4 shows a 3D representation of $S(\mathbf{q},t)$ in the scaling regime (at 75 min), before azimuthal averaging. Here and elsewhere the spike at $\mathbf{q}=0$ has been suppressed for clarity and the image has been smoothed to reduce noise. The ring at q_m corresponding to the peak of Fig. 3 is clearly apparent. However, on top of this ring hexagonal structure is evident. The random aggregation process thus spontaneously leads to broken symmetry: the rotational isotropy of the plane is reduced to triangular symmetry.

In particular, in the late, rapid stages of aggregation on high molarity substrates, where DLCA structures are apparent and where $S(q,t)$ scales as Eq. (2), the two-dimensional structure function $S(\mathbf{q},t)$ develops six small peaks symmetrically disposed upon the ring at q_m [Figs. 5(b,c)]. This sixfold structure in $S(\mathbf{q},t)$ is readily apparent for micrographs taken between 60 and 90 min. For $t\leqslant45$ min it is absent, apparently having not yet developed. For times later than those illustrated in Fig. 5 (data not shown) the small peaks decay in magnitude until eventually they are not apparent, as the ring in $S(\mathbf{q},t)$ shrinks to low q_m and becomes noisy (due to the small number of clusters), making it difficult to discern such detailed structure.

The angular autocorrelation functions $[c(\theta)]$ of the structure functions $S(\mathbf{q},t)$ for $q=q_m$ (evaluated from the angularly averaged structure functions of Fig. 3) were computed. These autocorrelation functions, shown in Fig. 6 for the cases of Fig. 5, confirmed that hexagonal structure appeared at that time at which scaling of $S(q,t)$ set in, thereafter gradually decaying into the noise. The obvious dipole character of $S(\mathbf{q},t)$ at 45 min is apparent in Fig. 6, whereas $c(\theta)$ for 60 min is almost purely hexapolar [the remnant dipole structure apparent in Fig. 5(b) occurs at $q<q_m$ and hence does not affect $c(\theta)$]. By 75 min the hexapolar component is less pronounced, but it is still significant (a quadrupole component of comparable amplitude is also present).

The tendency in real space to form a triangular lattice is not strong: the integrated volume under the peaks of $S(q,t)$ must be much less than that under the ring as q_m. While the most probable wavelength of the density modulation $(2\pi/q_m)$ *is* apparent in the micrographs (see the roughly equally spaced clusters of Fig. 2), the weakness of the triangular lattice makes it difficult to perceive any corresponding structure. Such hexagonal symmetry has never, to our knowledge, been reported before in experiments or computer simulations of cluster-cluster aggregation. Various lines argue strongly against it being an experimental artifact; we briefly review these.

These features of $S(\mathbf{q},t)$ are reproducible: they appear in all experiments for $CaCl_2$ concentrations above 0.5M, and in none of those below this concentration, suggesting their reality. Among possible causes of artifacts which we believe are eliminated is the residual mobility of the surface noted above, which leads to the recorded micrographs being quasirandomly selected portions of the monolayer. The sixfold symmetry seems not to be an artifact of the image processing: it is absent from early images and the orientation of the symmetry axes varies from image to image. Further, it seems unlikely that such features of $S(\mathbf{q},t)$ could result from statistical fluctuations in the system.

This question of fluctuations can be considered more quantitatively, on the assumption that intercluster effects underlie the hexagonal structure of $S(\mathbf{q},t)$. A single random 2D fractal will not be exactly circularly symmetric (indeed cluster-cluster aggregation is known to form anisotropic clusters [19]) and so its structure function must have extinctions at certain angles and hence angular intensity variations of order 100%. If N such clusters contribute to the total observed $S(\mathbf{q},t)$ then, assuming incoherent addition of the scattering due to individual clusters, one would expect angular fluctuations of order $1/\sqrt{N}$. To be accepted as significant, the magnitudes of the peaks of Fig. 4 should considerably exceed this value.

The number of clusters contained within the central 512×512 pixel portions of the micrographs [used in computing $S(\mathbf{q},t)$] are tabulated in Table I for various times, together with the consequent expected magnitude of the fluc-

tuations of $S(\mathbf{q},t)$, as well as the relative size of the observed peaks. It is apparent that the observed peaks at 60 and 75 min are statistically significant. As expected, the significance falls as time progresses and the cluster statistics become poorer. We believe that it is the concomitant increase in the inherent fluctuations which inhibits the observation of any traces of sixfold symmetry in $S(\mathbf{q},t)$ at times greater than 90 min in the present experiment. We further note that statistical fluctuations would not lead naturally to the symmetry evident in the sixfold peaks observed in our experiments and simulations.

B. Computer simulation

Although some relatively minor differences were apparent, the results of the simulations of 2D cluster-cluster aggregation (DLCA) were in general accord with the experimental results. In particular, as aggregation proceeded, a ring developed in $S(q,t)$ which showed scaling behavior as Eq. (2) at later stages (cf. [20]). In the scaling regime sixfold structure in $S(\mathbf{q},t)$ was apparent at q_m. Figure 7 shows the central 512×512 portion of the system at a relatively early stage in the simulation, together with a map of $S(\mathbf{q},t)$ (computed from the whole 1024×1024 system) which clearly shows the ring and the hexagonal symmetry. Most of the comments regarding the reliability of the experimental observations apply to the results of the simulations. In particular the features noted were observed for all simulations of DLCA, but not for RLCA. Further, the six symmetrically disposed peaks on the ring in $S(\mathbf{q},t)$ were again statistically significant (over 10 standard deviations in some cases). Again, as in the experiments, the peaks faded into statistical insignificance as time progressed and the cluster numbers fell.

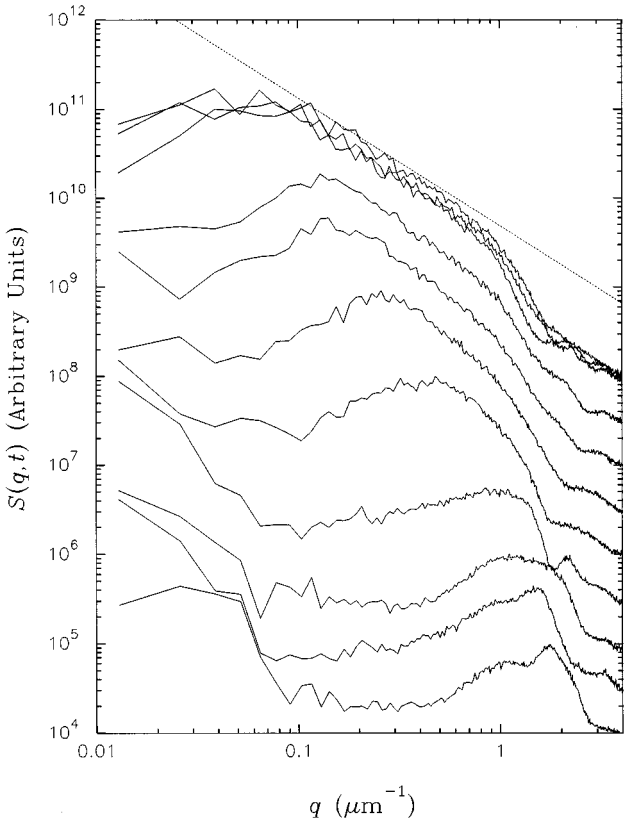

FIG. 3. The structure functions computed from the central 512×512 pixel portions of the micrographs, for the entire aggregation process, from 5 to 165 min, vertically displaced for clarity (except those in the gelling state). The dotted line indicates the power law scaling expected for DLCA ($d_f=1.44$); it clearly parallels the experimental $S(q,t)$ over part of the q range. Peaks [rings in $S(\mathbf{q},t)$] occur at all times, at q values designated q_m. As time progresses q_m falls.

The main difference between simulation and experiment was the much earlier appearance of scaling and sixfold symmetry in $S(\mathbf{q},t)$. Whereas in the experiments these features did not appear until the clusters became comparable in size with their separation, in the simulations the clusters were smaller than their separation at the onset of scaling. We believe that this difference arises from experimental problems: experimentally the particle-particle reaction kinetics were always reaction limited [6], a crossover to DLCA only occurring when large clusters formed, the increasing number of potential points of contact causing the probability of cluster-cluster bonding on contact to approach unity [7]. Scaling of $S(q,t)$ *only* occurs for DLCA, and so cannot occur experimentally until after this crossover. However, in the simulations the aggregation is diffusion limited from the start. As will be discussed below, scaling occurs when effective intercluster repulsions appear, leading to correlations. This occurs relatively earlier in the simulations.

IV. DISCUSSION

In the following, we largely concentrate upon the experimental situation, considering the simulations only where differences arise. We believe that these differences are of degree only, not of principle.

A. Mechanisms

What is the origin of the sixfold symmetry? Experimentally, the most obvious hypothesis would ascribe it to remnant electrostatic repulsion between clusters, due to inadequate screening by Ca^{2+} in the subphase. This explanation is untenable. Such repulsion would be stronger for lower salt concentrations, under which conditions RLCA is found [5]. However, the sixfold structure on the ring in $S(\mathbf{q},t)$ is only observed at *high* salt concentrations, i.e., for DLCA [5]. Furthermore, there is no repulsive interparticle potential in the simulations, yet the hexagonal structure emerges here, too.

TABLE I. The cluster numbers (N) and expected statistical fluctuations, expressed as a percentage of the magnitude of $S(q,t)$, together with the measured relative amplitudes of the sixfold peaks in the structure function.

Time (min)	N	Noise (%)	Amplitude (%)
45	3436	1.7	
60	1978	2.2	7
75	670	3.9	13
90	181	7.4	5

Thus the sixfold structure in $S(\mathbf{q},t)$ and the scaling of the structure function arise from spontaneous self-organization in the system.

Initiation of aggregation quenches the system into a nonequilibrium state. It is well established that, even in a steady state, macroscopic spatial patterns (dissipative structures) may emerge in such nonequilibrium systems [1,2]. The quench can be regarded as pushing the system over a threshold above which it is unstable to infinitesimal perturbations. Spatial structure then appears centered on the most unstable wave number, q_m, apparent here in both the ring of $S(\mathbf{q},t)$ and the sixfold structure. The six peaks lie at q_m, and so are linked to the spatial modulation of the density with that wave number. The temporal evolution of the system causes the steady decrease in q_m evident in Fig. 3.

Two possible general mechanisms for pattern formation can be considered [2], arising either from a conservation law or from competing interactions between elementary units. The present system apparently involves a crossover between the two. In particular, it appears [14] that the ring at q_m arises from different processes at early times and in the scaling regime. We briefly summarize the evidence which has led us to identify the mechanism in the latter regime [12,14,21].

q_m must relate to some characteristic length scale. From our two-dimensional images we can directly determine the two relevant length scales characterizing our aggregating monolayers [14]: the average cluster size and separation. We estimate the former as twice the average radius of gyration of the clusters, $2\langle R_g\rangle$, the latter as the average separation between the cluster centroids, $\langle x\rangle$ (both averages taken as medians to avoid problems of outliers and skew distributions). Both length scales are well characterized, as DLCA involves relatively monodisperse clusters uniformly spread throughout the system [22]. The variations of these lengths with time are shown in Fig. 8. It is apparent that, whereas initially we have small clusters which are comparatively widely separated, after 60 min we have large clusters which are rather closely packed. Indeed, just before gelation the average cluster size (~ 400 μm) greatly exceeds the cluster separation (~ 55 μm).

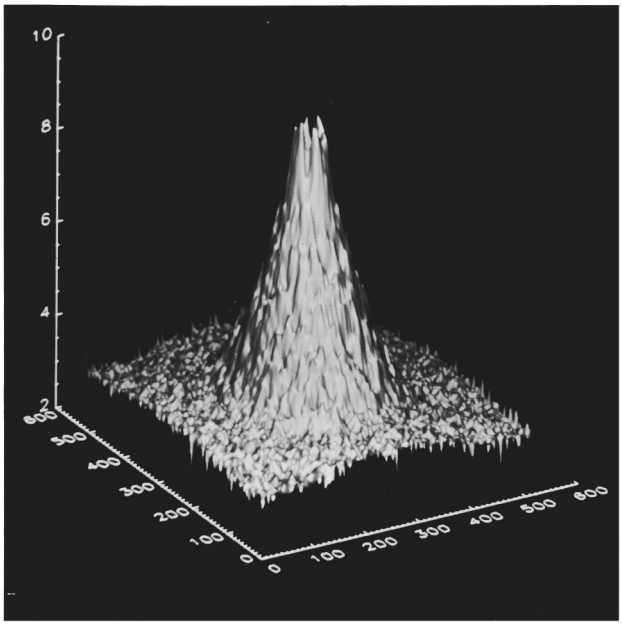

FIG. 4. A perspective view of $S(\mathbf{q},t)$ for the micrograph at 75 min [Fig. 2(b)]. The scales are arbitrary; q_x and q_y run from -3.29 to 3.29 $\mu\mathrm{m}^{-1}$. The ring at q_m is clear, as are the six peaks at that q.

How does q_m correlate with these length scales? Figure 8 includes the characteristic length scale of the density modulation in the system ($2\pi/q_m$), enabling comparisons to be drawn (see also [21]). At early times q_m is close to $2\langle R_g\rangle$: the ring in $S(\mathbf{q},t)$ is here due to growth of clusters at the expense of the monomer population, the low q fall off inside the ring arising from the finite cluster size. Thus the ring arises from mass conservation [23]. In DLCA cluster growth leads to the formation of depletion zones around the aggregates. These become larger as smaller clusters disappear by continued aggregation, eventually becoming comparable in size with the cluster separation [10,12]. The depletion zones are mutually exclusive, forcing a most probable length scale on the system, so that at later times ($t \geq 60$ min) q_m is determined by the intercluster separation, $\langle x\rangle$. While mass is still conserved, the driving force generating the structure at q_m is now the competition between these mutually exclusive depletion zones. As the structure coarsens through cluster growth, smaller clusters act as defects within the new, evolving pattern [cf. Fig. 2(b)]. Due to their relatively easy diffusion, they disappear by being mopped up by larger clusters, causing the structure to evolve into that appropriate to a larger cluster-cluster separation. The scaling of $S(q,t)$ as Eq. (2) arises from this self-organizing tendency of the depletion zones.

Scaling thus arises from effective intercluster interactions which spontaneously arise when the cluster size is comparable with, or greater than, the separation. Such interactions emerge naturally in DLCA: growth leads to mutually exclusive depletion zones around the clusters which provide an effective intercluster repulsion. It is these repulsions which lead to spatial correlations as the system evolves to an overall structure comprising nearly equally spaced fractal clusters.

The hexagonal structure appears in the scaling regime and at q_m, being a higher-order consequence of the self-organization which causes the scaling. The hexagonal symmetry depends upon development of depletion zones around the clusters. When small clusters are widely separated they exert no influence upon each other. Only when the structure at q_m is driven by competition between the clusters do the latter interact to impose order: large close-packed clusters must behave in a coherent fashion. When $q_m = 2\pi/\langle x\rangle$ the depletion zones around the clusters are evidently space-filling. In the absence of any symmetry-breaking influence such as gravity, their mutually exclusive character, acting in a plane, will then lead to a tendency for the basic entities (here clusters) to form a triangular lattice. One may think of optimally packed disks forming a triangular lattice. While softening the hard-disk interaction will reduce the global order of such a structure, it will not totally destroy it, particularly locally (see below).

Turning briefly to the results of the simulations, we recall that, in contrast to the experimental situation, scaling and the sixfold symmetry here appear while $2\langle R_g\rangle < \langle x\rangle$. However,

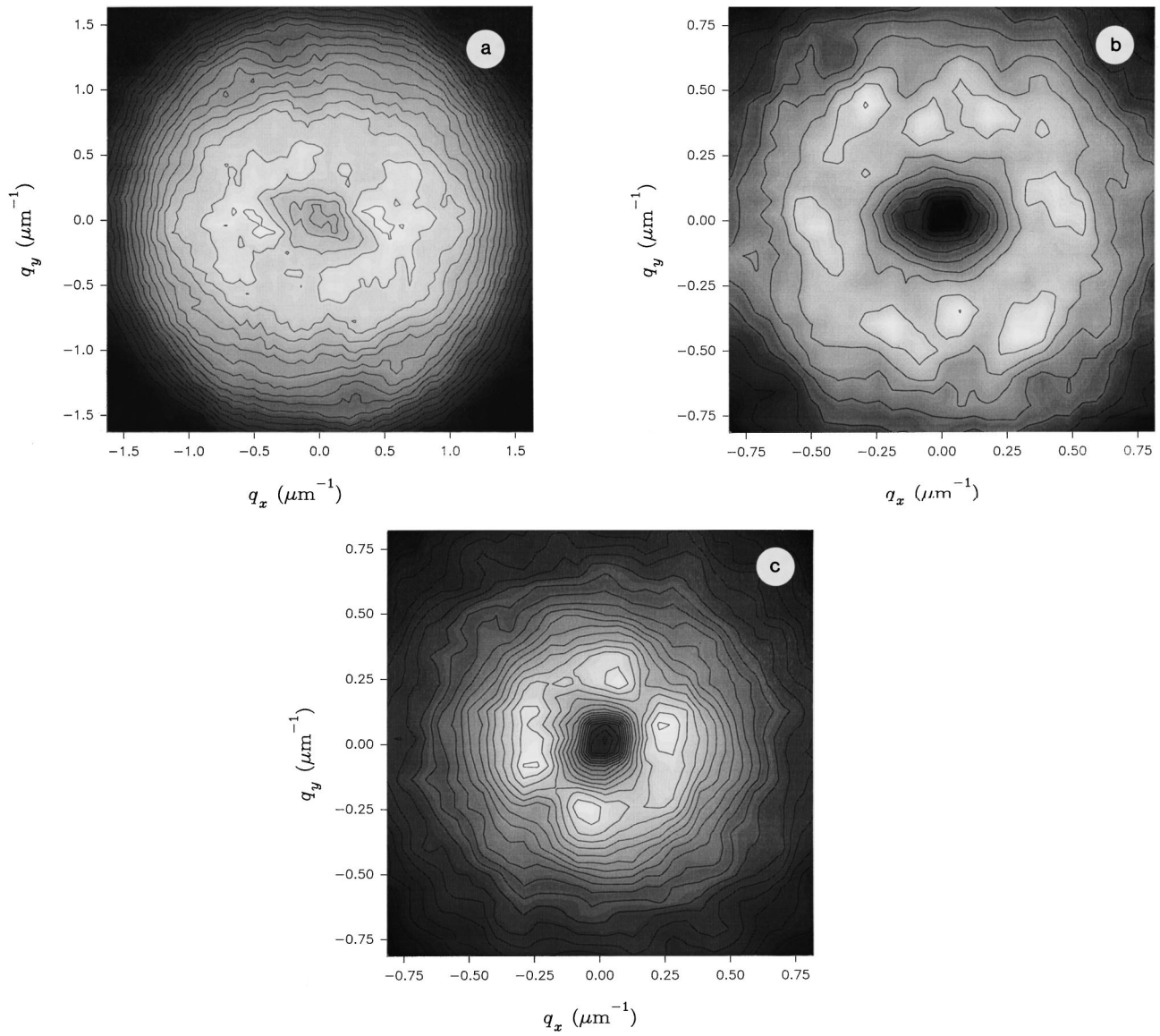

FIG. 5. Maps of the central region of the two-dimensional structure functions $S(\mathbf{q},t)$ for various micrographs: (a) for $t=45$ min; (b) for 60 min; (c) for 75 min. (For these maps the image is adjusted to use the full grey scale.)

the phenomena are still due to the mutually exclusive nature of the depletion zones around the clusters, characteristic of DLCA. Scaling and sixfold order in $S(\mathbf{q},t)$ can only occur when the aggregation is diffusion limited and the average diameter of the depletion zone is comparable with the cluster separation. The first condition shows why, experimentally, sixfold peaks only appear at the onset of the rapid growth phase: before that point the growth is basically reaction limited [7]. While DLCA is the intrinsic mechanism of aggregation in the simulations, depletion zones of the order of the cluster separation must also be present for local order to appear. The rms distance diffused by particles or clusters by time t is $\sim\sqrt{2Dt}$. At the very earliest times the depletion zones must be of small radius: sixfold order and scaling of $S(\mathbf{q},t)$ can only arise as t increases to $\langle x^2\rangle/2D$. This estimate exactly agrees with results from the present simulations.

It has been suggested [16] that structure function scaling in colloidal aggregation implies a progressive ''hardening'' of the radial distribution function of the clusters (i.e., a tendency towards a step function). We do not observe this. Figure 9 shows pair correlation functions of the centroids of the clusters, in the scaling regime of the experiments. The functions are scaled laterally by $\langle x\rangle$ and vertically to equal depths at the minimum to facilitate comparison. Despite the rather large fluctuations evident at the later times, they clearly superimpose essentially exactly, indicating that the shape of the effective intercluster potential remains constant through the scaling phase of the aggregation process.

B. Local order

The appearance of local order in the regime in which $S(q,t)$ scales is comprehensible in terms of the mechanism sketched above. For objects in a plane, an effective repulsive intercluster potential which is of long range will lead to a triangular organization of the objects. For a purely nearest-neighbor interaction, as here, and for a relatively ''soft'' potential this organization will be relatively weak, as observed:

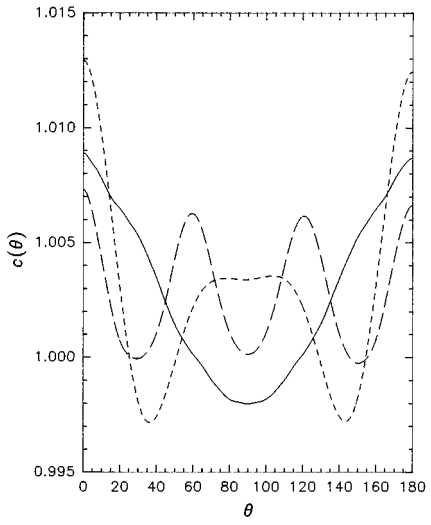

FIG. 6. Angular autocorrelation functions of $S(\mathbf{q}_m,t)$ for 45 (continuous line), 60 (long dashed), and 75 min (short dashed) θ is in degrees. See text for discussion.

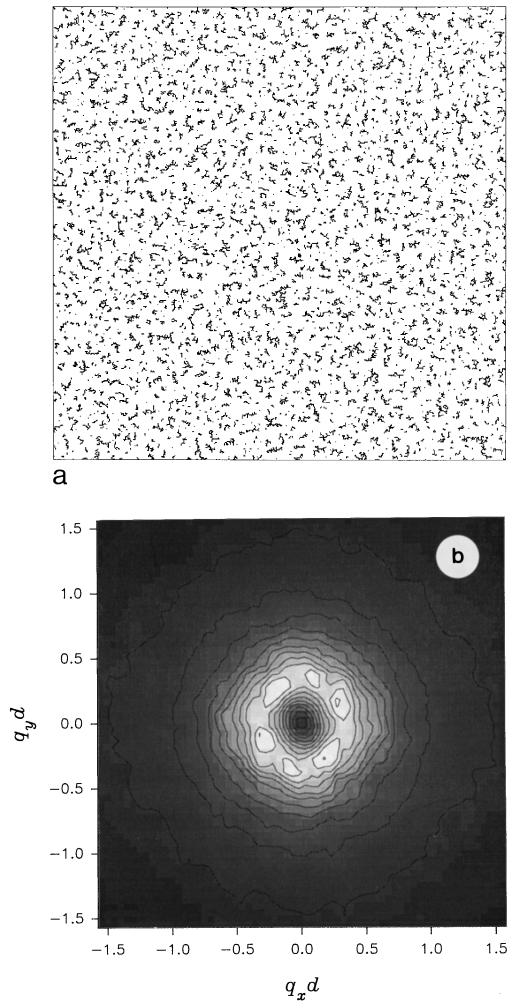

FIG. 7. Typical results from computer simulations. (a) The central 512×512 portion of a 1024×1024 system undergoing DLCA. (b) The map of the central part of $S(\mathbf{q},t)$ corresponding to the whole system (d is the lattice constant of the real space system).

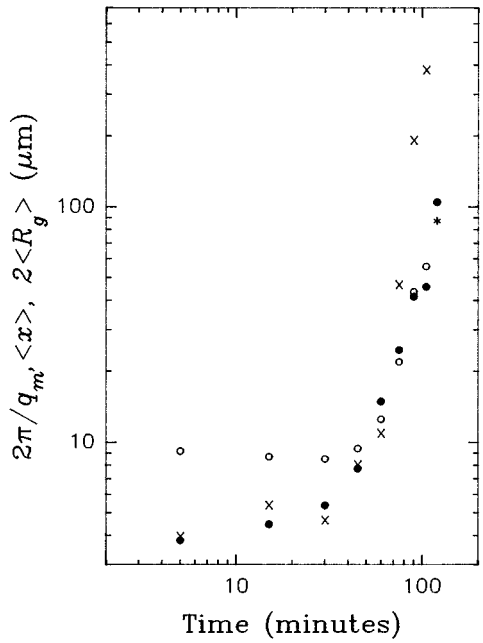

FIG. 8. Characteristic length scales for the experiment, as functions of time: $\langle x\rangle$ (○), $2\langle R_g\rangle$ (×), and $2\pi/q_m$ (●). The point ⋆ at 120 min derives from the inside of the depletion zone in the gelled state [21].

the intercluster separation is quite well-defined, but the local tendency to a triangular structure is not strong, as noted in Sec. III.

Such *local* quasicrystalline order is known from liquids. For a liquid the conventional diffraction pattern resembles a Debye-Scherrer ring, at a radius governed by the particle-particle separation, reflecting the global disorder of the system. However, if the diameter of the illuminating beam is systematically reduced, a point is reached at which peaks appear at points corresponding to the crystalline lattice. In this situation the beam is illuminating, and so scattering occurs from, a single domain (or at most a very few) over which local order persists. Ackerson *et al.* [24] have beautifully demonstrated this point for a colloidal liquid. As their sample was progressively moved nearer to the focus of the illuminating laser beam, rather noisy but clearly apparent peaks appeared. The key point is that the solid and liquid states had similar *local* structures and densities, differing in that the defects in the liquid phase led to global disorder and a global density lower than in the solid.

We believe that the present systems comprise such a 2D liquid phase, with clusters as ''atoms.'' In such a phase intercluster order can only be expected when the range of the intercluster interaction is comparable with the cluster separation, as found here.

Is the local order a consequence of the fractal nature of the clusters, or the other way around? Order can only arise in a coarsening process when the range of influence of the individual entities is of the order of their mutual separation. In the absence of real long-range forces, this implies that the clusters can exert an indirect long-ranged influence on each other. Experimentally this only occurs when they have grown to be larger than their average separation; in the simulations, when the diffusion distance scale exceeds this sepa-

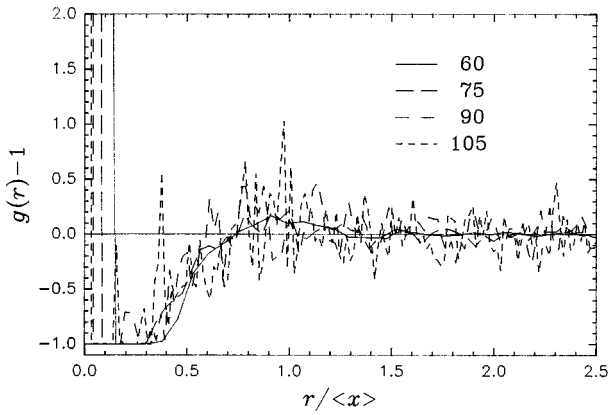

FIG. 9. Pair correlation functions for centroids of clusters in the experimental images, after the onset of scaling (times as legend). r is scaled by $\langle x \rangle$, and the functions are normalized to a common minimum value.

ration. The clusters are, however, fractal both before and after the onset of scaling, that is the crossover to rapid aggregation [7]. It is evident that the order discussed here is a direct outgrowth of the fractal nature of the aggregates; the size of compact quasicircular objects can never exceed their center-to-center separation.

C. General

In previous publications [13,14] we have discussed various scaling aspects of the present experimental systems, including topological and metrical properties of the ensemble of clusters. Some of these might be thought to relate to the present results, and so we briefly discuss several points.

A starting point is consideration of the nearest-neighbor clusters. The distribution of the numbers of nearest neighbors (n) is relevant to the question of order.

We first note that the clusters formed in DLCA do not form a random spatial distribution of points in the plane: the second central moment of $P(n)$, μ_2, is significantly less (~ 1.25 for DLCA [13,14]) than that of such a random array ($=1.84$ [25]). This confirms that there is some degree of intercluster order in the DLCA system. We further note that μ_2 for DLCA does not evolve with time [13,14], whereas the sixfold order does develop as time progresses.

We emphasize that the tendency of objects (here clusters) in a plane to have, on average, six nearest neighbors in no way underlies the present reduction in rotational symmetry. The sixfold structure of $S(\mathbf{q},t)$ relates to the spatial distribution of the clusters in the plane, whereas Euler's theorem [26] demands that the mean coordination number of a 2D array of points *must* equal 6, irrespective of that distribution. The two facts thus cannot be connected. However, the experimental $P(n)$ do peak quite strongly at $n=6$, [14] which might be interpreted as underlying the sixfold symmetry. But this is also true for RLCA [14], for which case we never observe scaling or sixfold symmetry in $S(\mathbf{q},t)$. Further, $P(6)$ is, within uncertainties, constant throughout the DLCA process, whereas the sixfold peaks of $S(\mathbf{q},t)$ only appear at a time when $S(q,t)$ starts to scale. We conclude that the symmetry breaking is not associated with a mean or modal $n=6$.

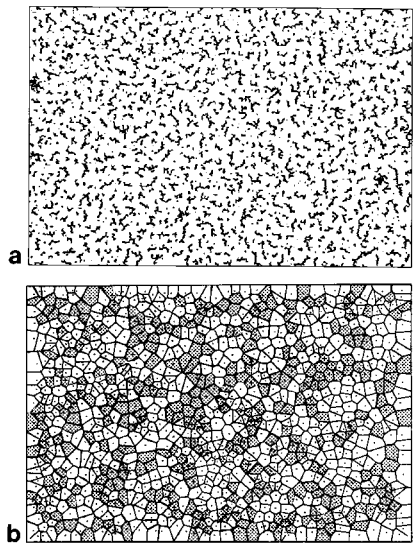

FIG. 10. An illustration of the topological order for a typical DLCA micrograph (75 min): original image (a) and the corresponding Voronoi diagram (b), in which the points indicate the centroids of the clusters.

Figure 10 shows a micrograph for which $S(\mathbf{q},t)$ exhibited sixfold symmetry and the corresponding Voronoi diagram, partitioning the plane into areas (called cells) closer to a given point than to any other point in the system [26]. In the present context ''points'' are cluster centroids, and the number of sides of a Voronoi cell equals the cluster coordination number. Cells with six sides are shaded for emphasis: in 2D defects correspond to $n \neq 6$ [27]. It is clear that the ordered regions indicated by the shaded cells are neither extensive nor very correlated, confirming that such topological order cannot underlie the present metrical order.

Finally, it might be thought that sixfold symmetry in $S(\mathbf{q},t)$ should be associated with significant bond-orientational correlations. We believe that this is not so. Such

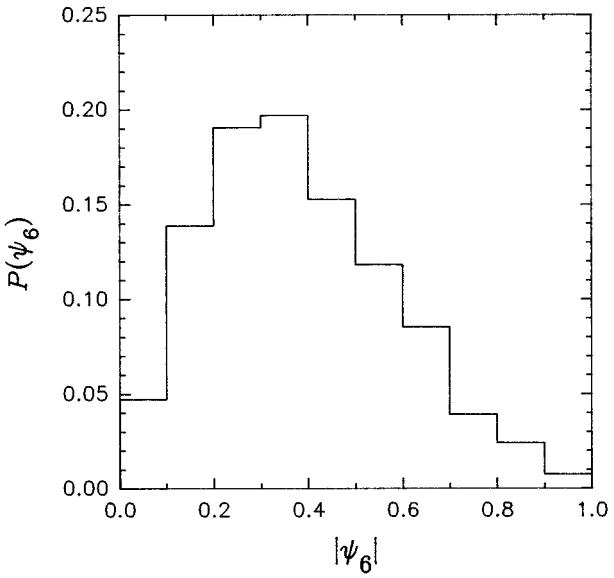

FIG. 11. The distribution of the bond-orientational order parameter $|\psi_6|$ for the experimental image at 60 min (statistics are worse at later times). See text for discussion.

order is defined via a bond-orientational order parameter, defined for cluster i located at $\mathbf{r}_i$ as [28]

$$\psi_6(\mathbf{r}_i) = \sum_j e^{i6\theta_{ij}}, \tag{3}$$

where θ_{ij} is the angle of the ''bond'' between cluster i and one of its j nearest neighbors (here simply the centroid to centroid displacement). For a perfect 2D triangular lattice ψ_6 is unity for all atoms, being spatially correlated over the entire lattice. As the lattice melts $\langle|\psi_6|\rangle$ falls and the correlation length decreases, particularly in the fluid state [27]. In the 2D liquid $P(|\psi_6|)$ becomes broad, rather than being concentrated at >0.75, as in the solid [27].

Figure 11 shows a typical example of $P(|\psi_6|)$ determined from the present experimental data. It is clearly very broad indeed. Neither the distribution of $|\psi_6|$ nor its average value (~ 0.4) vary significantly with time. In particular, there is no significant change at the onset of scaling and the appearance of hexagonal structure in $S(\mathbf{q},t)$. The observed $P(|\psi_6|)$ clearly corresponds to a system which is far from a crystalline or hexatic state; long-range correlations of ψ_6 cannot be expected, and are not found. The probability of $|\psi_6|$ exceeding 0.75, which approaches unity in a solid [27], is ~ 0.05 for our system. This seems entirely consistent with the *weak* local order implied by the small sixfold peaks in $S(\mathbf{q},t)$. However, the liquid state, which involves the absence of both long-range translational and bond-orientational order is, as we have seen, entirely consistent with *local* sixfold symmetry [24].

V. CONCLUSIONS

It has been demonstrated that, both experimentally and in simulations, diffusion limited cluster-cluster aggregation in 2D leads to local triangular order in the cluster positions. The degree of this order is not large; the clusters appear to form a 2D liquid. The order arises at the same time as the ''spinodal-like'' scaling of the structure function sets in, and at the same q as the scaling peak in the structure function. It is therefore apparent that this symmetry breaking is intimately connected with the modulation of the density which underlies the scaling. The two phenomena both originate in the effective long-range intercluster repulsion due to the mutually exclusive depletion zones surrounding each cluster in DLCA.

The present results raise various questions. Does the sixfold symmetry persist throughout the aggregation process, or do the chaotic dynamics underlying the fractal structure finally dominate the self-organizing influences and destroy it? If not, does the symmetry persist into the gelled state? Further experiments (real or numerical) with better cluster number statistics are required to answer these and other questions.

ACKNOWLEDGMENTS

This work was supported by the EPSRC. M.B.J.H. thanks DENI for financial support. We thank V. Degiorgio for helpful discussions.

[1] J.S. Kirkaldy, Rep. Prog. Phys. **55**, 723 (1992).
[2] M.C. Cross and P.C. Hohenberg, Rev. Mod. Phys. **65**, 851 (1993).
[3] G. Nicolis and I. Prigogine, *Self-Organization in Nonequilibrium Systems* (Wiley, New York, 1986).
[4] E.g., A. Fuchs, J.A.S. Kelso, and H. Haken, Int. J. Bifurc. Chaos **2**, 917 (1992).
[5] D.J. Robinson and J.C. Earnshaw, Phys. Rev. A **46**, 2045 (1992).
[6] D.J. Robinson and J.C. Earnshaw, Phys. Rev. A **46**, 2055 (1992).
[7] D.J. Robinson and J.C. Earnshaw, Phys. Rev. A **46**, 2065 (1992).
[8] R. Jullien and R. Botet, *Aggregation and Fractal Aggregates* (World Scientific, Singapore, 1987); T. Vicsek, *Fractal Growth Phenomena* (World Scientific, Singapore, 1992).
[9] P. Meakin, Phys. Scr. **46**, 295 (1992).
[10] M. Carpineti and M. Giglio, Phys. Rev. Lett. **68**, 3327 (1992).
[11] J. Bibette, T.G. Mason, H. Gang, and D.A. Weitz, Phys. Rev. Lett. **69**, 981 (1992).
[12] D.J. Robinson and J.C. Earnshaw, Phys. Rev. Lett. **71**, 715 (1993).
[13] J.C. Earnshaw and D.J. Robinson, Phys. Rev. Lett. **72**, 3682 (1994).
[14] J.C. Earnshaw and D.J. Robinson, Physica A **214**, 23 (1995).
[15] A.J. Hurd, J. Phys. A **18**, L1055 (1985).
[16] F. Sciortino and P. Tartaglia, Phys. Rev. Lett. **74**, 282 (1995).
[17] M. Carpineti, M. Giglio, and V. Degiorgio, Phys. Rev. E **51**, 590 (1995).
[18] J.S. Langer, in *Solids Far From Equilibrium,* edited by C. Godrèche (Cambridge University Press, Cambridge, 1992), p. 297.
[19] R. Botet and R. Jullien, J. Phys. A **19**, L907 (1986).
[20] M.D. Haw, M. Sievwright, W.C.K. Poon, and P.N. Pusey, Physica A **217**, 231 (1995).
[21] J.C. Earnshaw and D.J. Robinson, Nuovo Cimento **16D**, 1141 (1994).
[22] P. Meakin, T. Vicsek, and F. Family, Phys. Rev. B **31**, 564 (1985).
[23] G. Banfi, V. Degiorgio, A.R. Rennie, and J.G. Barker, Phys. Rev. Lett. **69**, 3401 (1992).
[24] N.A. Clark, B.J. Ackerson, and T.W. Taylor, J. Phys. (Paris) **46**, C3-137 (1985).
[25] G. Le Caër and R. Delannay, J. Phys. A **26**, 3931 (1993).
[26] F.P. Preparata and M.I. Shamos, *Computational Geometry* (Springer-Verlag, New York, 1985), Chap. 4.
[27] E.g., M.A. Glazer and N.A. Clark, Adv. Chem. Phys. **83**, 543 (1993).
[28] E.g., C.A. Murray, W.O. Springer, and R.A. Wenk, Phys. Rev. B **42**, 688 (1990).